Theoretical Investigation of C−H/Olefin Coupling Catalyzed by Zirconium(IV) Complexes

Siwei Bi and Zhenyang Lin*

Department of Chemistry and Open Laboratory of Chirotechnology of the Institute of Molecular Technology for Drug Discovery and Synthesis, The Hong Kong University of Science and Technology, Clear Water Bay, Kowloon, Hong Kong

Richard F. Jordan*

Department of Chemistry, The University of Chicago, 5735 South Ellis Avenue, Chicago, Illinois 60637

Received May 6, 2004

Density functional theory calculations at the B3LYP level have been performed to investigate the mechanism of the zirconocene-catalyzed addition of the ortho C−H bond of α-picoline to propene to produce 2-Me-6-^{i}Pr-pyridine. The computational results support the proposed mechanism, which involves (i) 2-Me-pyridine dissociation from [Cp_2Zr(2-Me-6-pyridyl)(2-Me-pyridine)]$^+$ followed by the insertion of propene into the Zr−C bond of the η^2-pyridyl complex $Cp_2Zr(\eta^2$-2-Me-6-pyridyl)$^+$ (**1**) to yield the azametallacycle $Cp_2Zr\{\eta^2$-*C*,*N*-CH_2CHMe-(2-Me-6-pyridyl)$\}^+$ (**2**), (ii) hydrogenolysis of **2** to produce Cp_2Zr(H)(2-Me-6-^{i}Pr-pyridine)$^+$ (**3**), (iii) ligand substitution of **3** by α-picoline to release 2-Me-6-^{i}Pr-pyridine and form Cp_2Zr(H)(2-Me-pyridine)$^+$ (**4**), and (iv) C−H activation of **4** to release H_2 and regenerate **1**. Consistent with the experimental results, the 2-Me-pyridine dissociation from [Cp_2Zr(2-Me-6-pyridyl)(2-Me-pyridine)]$^+$ followed by the propene insertion of **1** and the hydrogenolysis of **2** are calculated to be the rate-determining steps. The calculations provide new insights into the role of the cocatalyst H_2, the origin of the regioselectivity of the C−H activation and insertion steps, and the preference for α-picoline/propene coupling over propene hydrogenation.

Introduction

Transition metal-catalyzed additions of C−H bonds to olefins (eq 1)[1] provide potentially economic and versatile approaches to the formation of C−C bonds.[2] A general mechanism for late transition metal catalysts involves C−H oxidative addition, olefin insertion, and reductive elimination of the product (Scheme 1).[3] In

Scheme 1

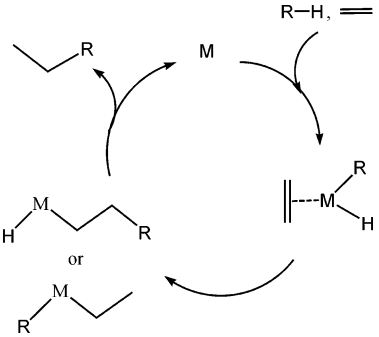

contrast, for d^0 early transition metal catalysts, which cannot undergo oxidative addition, the mechanism normally involves σ-bond metathesis processes.[4]

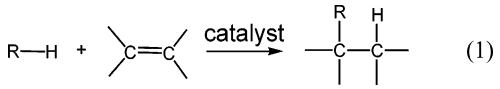

(1)

To date, few theoretical calculations on these kinds of addition reactions have been reported.[5] In this paper, we describe computational studies of the zirconocene-catalyzed addition of the ortho C−H bond of α-picoline to propene (eq 2) reported by Jordan and coworkers.[6,7] The objectives of this computational work were to understand the general reaction mechanism, the role of H_2, and the origin of the selectivity for the

* To whom correspondence should be addressed. E-mail: chzlin@ust.hk and rfjordan@uchicago.edu.

(1) (a) Shilov, A. E.; Shul'pin, G. B. *Chem. Rev.* **1997**, *97*, 2879. (b) Ritleng, V.; Sirlin, C.; Pfeffer, M. *Chem. Rev.* **2002**, *102*, 1731.

(2) (a) Jones, W. D.; Feher, F. J. *Acc. Chem. Res.* **1989**, *22*, 91. (b) Arndtsen, B. A.; Bergman, R. G.; Mobley, T. A.; Peterson, T. H. *Acc. Chem. Res.* **1995**, *28*, 154. (c) Dyker, G. *Angew.* Chem., Int. Ed. **1999**, *38*, 1698. (d) Guari, Y.; Sabo-Etienne, S.; Chaudret, B. *Eur. J. Inorg. Chem.* **1999**, 1047. (e) Kakiuchi, F.; Murai, S. *Acc. Chem. Res.* **2002**, *35*, 826.

(3) (a) Jones, W. D.; Feher, F. J. *J. Am. Chem. Soc.* **1984**, *106*, 1650. (b) Kakiuchi, F.; Sekine, S.; Tanaka, Y.; Kamatani, A.; Sonoda, M.; Chatani, N.; Murai, S. *Bull. Chem. Soc. Jpn.* **1995**, *68*, 62. (c) Kakiuchi, F.; Yamamoto, Y.; Chatani, N.; Murai, S. *Chem. Lett.* **1995**, 681. (d) Kakiuchi, F.; Sato, T.; Tsujimoto, T.; Yamauchi, M.; Chatani, N.; Murai, S. *Chem. Lett.* **1998**, 1053. (e) Lewis, L. N.; Smith, J. F. *J. Am. Chem. Soc.* **1986**, *108*, 2728. (f) Murai, S.; Kakiuchi, F.; Sekine, S.; Tanaka, Y.; Kamatani, A.; Sonoda, M.; Chatani, N. *Nature* **1993**, *366*, 529. (g) Fujii, N.; Kakiuchi, F.; Chatani, N.; Murai, S. *Chem. Lett.* **1996**, 939. (h) Fujii, N.; Kakiuchi, F.; Yamada, A.; Chatani, N.; Murai, S. *Chem. Lett.* **1997**, 425. (l) Fujii, N.; Kakiuchi, F.; Yamada, A.; Chatani, N.; Murai, S. *Bull. Chem. Soc. Jpn.* **1998**, *71*, 285.

10.1021/om0496784 CCC: $27.50
Publication on Web 09/08/2004

Markovnikov C−H addition product, and to probe why competing processes such as activation of the picoline methyl C−H bonds and hydrogenation of propene are disfavored.

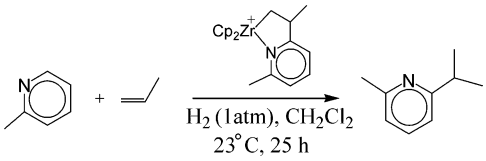

(2)

Computational Details

Geometry optimizations were performed using density functional theory calculations at the Becke3LYP (B3LYP) level.[8] In one of our previous studies, the energetics and structures calculated from B3LYP calculations have been found to give reliable results on reaction mechanisms involving early transition metals.[9] Frequency calculations at the same level of theory have also been performed to identify all stationary points as minima (zero imaginary frequency) or transition states (one imaginary frequency). The effective core potentials (ECPs) of Hay and Wadt with a double-ζ valence basis set (LanL2DZ)[10] were used to describe the Zr and Si atoms. The 6-31G basis set was used for all other atoms.[11] Polarization functions were also added for Si ($\zeta_d = 0.262$) and those atoms directly involved in bond-forming and bond-breaking processes [N ($\zeta_d = 0.864$), C ($\zeta_d = 0.600$), and H ($\zeta_p = 1.100$)]. All calculations were performed with the Gaussian 98 software package.[12]

In Figure 1 and the following figures that contain potential energy profiles, reaction free energies (kcal/mol) and reaction energies (kcal/mol, in parentheses) calculated at the B3LYP level are presented. The reaction free energies and reaction energies are similar in cases where number of reactant and product molecules is equal, e.g., one-to-one or two-to-two transformations, but differ significantly for one-to-two or two-to-one transformations because of the entropy contribution. In this paper, reaction free energies are used to analyze the reaction mechanism.

Results and Discussion

Reaction Mechanisms. Jordan and co-workers[6] showed that the reaction in eq 2 proceeds by the mechanism in Scheme 2. Overall, the catalytic cycle can be divided into four major steps. Starting with the η^2-pyrid-2-yl complex **1**, the first step (I) is the insertion of propene into the Zr−C bond to form azazirconacycle **2**. Complex **2** reacts with H_2 to give **3** via σ-bond metathesis (II). A subsequent ligand substitution step (III) yields **4** and releases the disubstituted pyridine product. Finally, release of H_2 via σ-bond metathesis (step IV) regenerates **1** and H_2 and completes the cycle.

In Scheme 2, H_2 acts as a cocatalyst; that is, it is required for the reaction to proceed, but it is not consumed. An alternative possible mechanism that does not involve H_2 is shown in Scheme 3. In Scheme 3, intermediate **2** reacts directly with α-picoline via a σ-bond metathesis transition state to regenerate **1** and release the disubstituted pyridine product.

Calculated Energy Profile for Scheme 3. The calculated potential energy profile for Scheme 3 is shown in Figure 1a. The insertion of propene into the Zr−C bond in **1** occurs via propene adduct **5** and transition state **TS1**. Adduct **5** is higher in free energy than **1** and free propene due to the entropy contribution. The activation free energy for propene insertion is 19.85 kcal/mol. The geometry of **TS1** is shown in Figure 2. In **TS1** the Zr−C3 σ-bond and the C1−C2 π-bond are partially broken, and the new σ-bonds Zr−C1 and C2−C3 are partially formed. The reaction of **1** with propene giving **2** is thermodynamically favorable, although the entropy is decreased. The stability of **2** is a result of the net energy gained from breaking the C1−C2 π-bond and forming the C2−C3 σ-bond. In adduct **5**, the coordination of olefin is from the C-side of the pyridyl ligand. N-side coordination of the olefin is also possible but will be disfavored by steric interactions between the propene methyl group and the pyridyl methyl group. Additionally, the N-side adduct must isomerize to the C-side adduct to undergo olefin insertion. The N-side isomer is calculated to be 0.94 kcal/mol higher in free energy than the C-side isomer, and therefore, we did not consider this species further.

There are two pathways for the direct reaction of **2** with α-picoline to yield **1** and the addition product, which differ in the orientation of the α-picoline ligand (see **TS2** and **TS3** in Figure 1a). In transition state **TS2**, the α-picoline nitrogen (N1) is coordinated to Zr, while in transition state **TS3** the α-picoline nitrogen points away from the metal center (Figure 2). Intrinsic reaction coordinate (IRC) calculations confirmed that no intermediates exist from **TS3** (or **TS2**) to **1** and the addition product.

Figure 2 shows the detailed structures of **TS2** and **TS3**. Both are four-center−four-electron σ-bond metathesis transition states. The Zr−H, C1−H, and C2−H distances indicate that the migrating H atom has strong interactions with the metal center and C1 and C2 in

(4) (a) Thompson, M. E.; Baxter, S. M.; Bulls, A. R.; Burger, B. J.; Nolan, M. C.; Santarsiero, B. D.; Schaefer, W. P.; Bercaw, J. E. *J. Am. Chem. Soc.* **1987**, *109*, 203. (b) Burger, B. J.; Thompson, M. E.; Cotter, W. D.; Bercaw, J. E. *J. Am. Chem. Soc* **1990**, *112*, 1566. (c) Sola, M.; Ziegler, T. *Organometallics* **1996**, *15*, 2611. (d) Woo, T. K.; Margl, P. M.; Ziegler, T. *Organometallics* **1997**, *16*, 3454. (e) Gilbert, T. M.; Hristov, I.; Ziegler, T. *Organometallics* **2001**, *20*, 1183. (f) Hristov, I. H.; Ziegler, T. *Organometallics* **2003**, *22*, 3513. (g) Eisenstein, O.; Maron, L. *J. Organomet. Chem.* **2002**, *647*, 190. (h) Maron, L.; Eisenstein, O. *J.* Am. Chem. Soc. **2001**, *123*, 1036. (i) Perrin, L.; Maron, L.; Eisenstein, O. *Inorg. Chem.* **2002**, *41*, 4355. (j) Sadow, A. D.; Tilley, T. D. *Organometallics* **2003**, *22*, 3577.

(5) Oxgaard, J.; Goddard, W. A., III. *J. Am. Chem. Soc.* **2004**, *126*, 442.

(6) Jordan, R. F.; Taylor, D. F. *J. Am. Chem. Soc.* **1989**, *111*, 778.

(7) (a) Jordan, R. F.; Guram, A. S. *Organometallics* **1990**, *9*, 2116. (b) Guram, A. S.; Jordan, R. F.; Taylor, D. F. *J. Am. Chem. Soc.* **1991**, *113*, 1833. (c) Rodewald, S.; Jordan, R. F. *J. Am. Chem. Soc.* **1994**, *116*, 4491. (d) Dagorne, S.; Rodewald, S.; Jordan, R. F. *Organometallics* **1997**, *16*, 5541.

(8) (a) Becke, A. D. *J. Chem. Phys.* **1993**, *98*, 5648. (b) Miehlich, B.; Savin, A.; Stoll, H.; Preuss, H. *Chem. Phys. Lett.* **1989**, *157*, 200. (c) Lee, C.; Yang, W.; Parr, G. *Phys. Rev.* **1988**, *B37*, 785.

(9) Liu, D.; Lin, Z. *Organometallics* **2002**, *21*, 4750.

(10) (a) Hay, P. J.; Wadt, W. R. *J. Chem. Phys.* **1985**, *82*, 270. (b) Wadt, W. R.; Hay, P. J. *J. Chem. Phys.* **1985**, *82*, 284. (c) Hay, P. J.; Wadt, W. R. *J. Chem. Phys.* **1985**, *82*, 299.

(11) Hariharan, P. C.; Pople, J. A. *Theor. Chim. Acta* **1973**, *28*, 213.

(12) Frisch, M. J.; Trucks, G. W.; Schlegel, H. B.; Scuseria, G. E.; Robb, M. A.; Cheeseman, J. R.; Zakrzewski, V. G.; Montgomery, J. A., Jr.; Stratmann, R. E.; Burant, J. C.; Dapprich, S.; Millam, J. M.; Daniels, A. D.; Kudin, K. N.; Strain, M. C.; Farkas, O.; Tomasi, J.; Barone, V.; Cossi, M.; Cammi, R.; Mennucci, B.; Pomelli, C.; Adamo, C.; Clifford, S.; Ochterski, J.; Petersson, G. A.; Ayala, P. Y.; Cui, Q.; Morokuma, K.; Malick, D. K.; Rabuck, A. D.; Raghavachari, K.; Foresman, J. B.; Cioslowski, J.; Ortiz, J. V.; Stefanov, B. B.; Liu, G.; Liashenko, A.; Piskorz, P.; Komaromi, I.; Gomperts, R.; Martin, R. L.; Fox, D. J.; Keith, T.; Al-Laham, M. A.; Peng, C. Y.; Nanayakkara, A.; Gonzalez, C.; Challacombe, M.; Gill, P. M. W.; Johnson, B. G.; Chen, W.; Wong, M. W.; Andres, J. L.; Head-Gordon, M.; Replogle, E. S.; Pople, J. A. *Gaussian 98*, revision A.9; Gaussian, Inc.: Pittsburgh, PA, 1998.

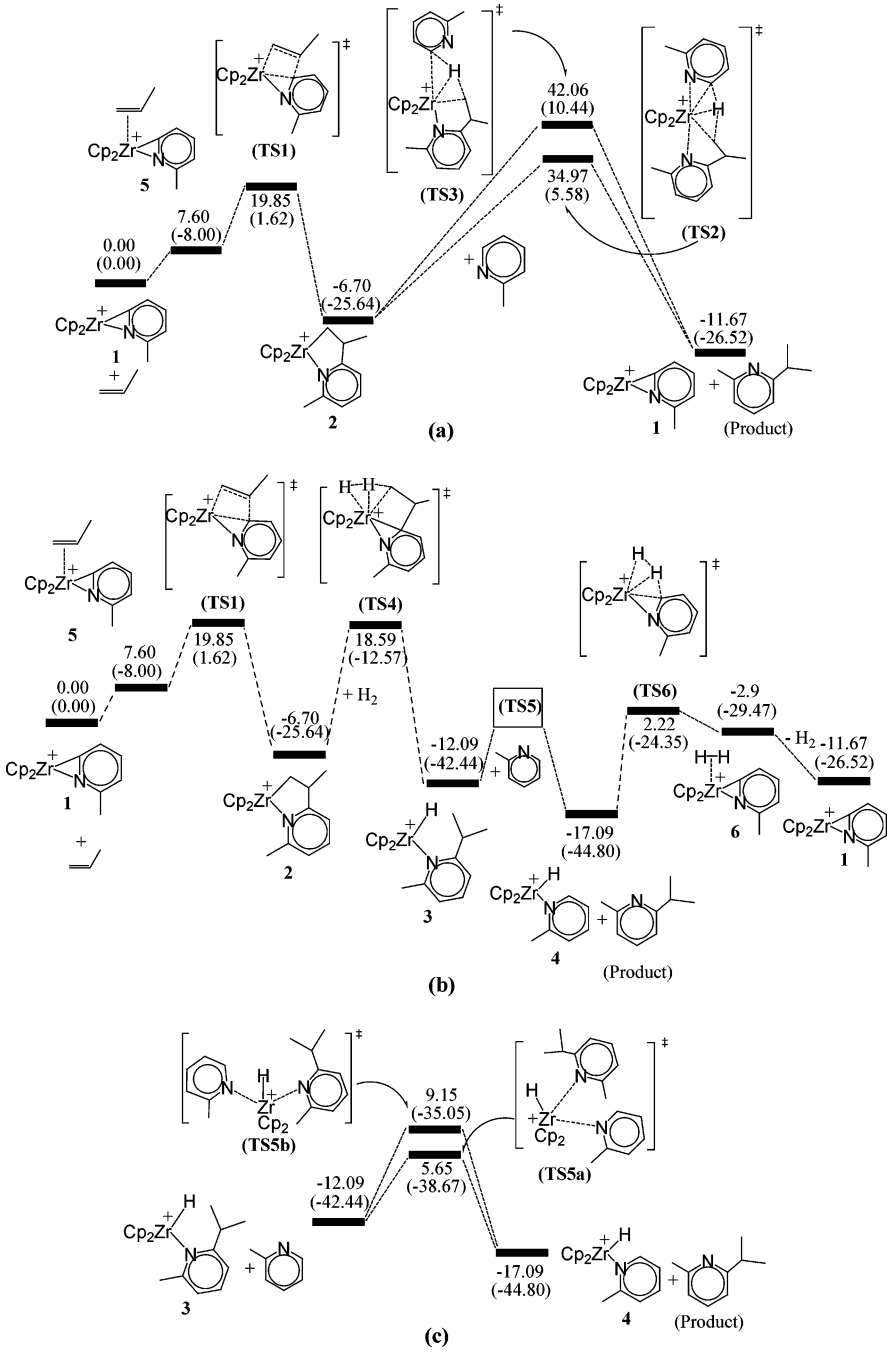

Figure 1. (a) Energy profile for the catalytic cycle shown in Scheme 3. (b) Energy profile for the catalytic cycle shown in Scheme 2. (c) Energy profile for the ligand substitution reaction of **3** → **4**. The calculated reaction free energies and reaction energies (in parentheses) are given in kcal/mol.

both **TS2** and **TS3**. In **TS2**, the incoming α-picoline is strongly N-coordinated to Zr (Zr−N1 distance 2.253 Å), and the departing disubstituted pyridine is not N-bound (Zr−N2 distance > 4 Å). The short Zr−N1 distance suggests that the new Zr−N bond is almost completely formed in the transition state. In the X-ray structure of $[Cp_2Zr(\eta^2\text{-pyridyl})PMe_3]^+$, the Zr−N bond is 2.21 Å.[13] In contrast, in **TS3**, the incoming α-picoline is bound to Zr only through the ortho C−H bond, while the departing pyridine is weakly N-bound (Zr−N2 distance 2.537 Å). **TS2** is significantly more stable than **TS3** due to the stronger α-picoline coordination. However, the activation energies via **TS2** and **TS3** are both very high (41.67 and 48.86 kcal/mol, respectively, from **2**), implying that neither pathway will be kinetically favorable.

Calculated Energy Profile for Scheme 2. Figure 1b shows the potential energy profile for Scheme 2, in which H_2 acts as a cocatalyst. The propene insertion of **1** to generate **2** was discussed above. The reaction of **2** with H_2 proceeds via the four-center−four-electron transition state **TS4** (Figure 2) to afford **3**. This step is thermodynamically favorable, although the entropy is decreased ($\Delta G = -5.39$ kcal/mol). The enthalpic driving force for this step is formation of the Zr−H bond, which

(13) Jordan, R. F.; Taylor, D. F.; Baenziger, N. C. *Organometallics* **1990**, *9*, 1546.

Scheme 2

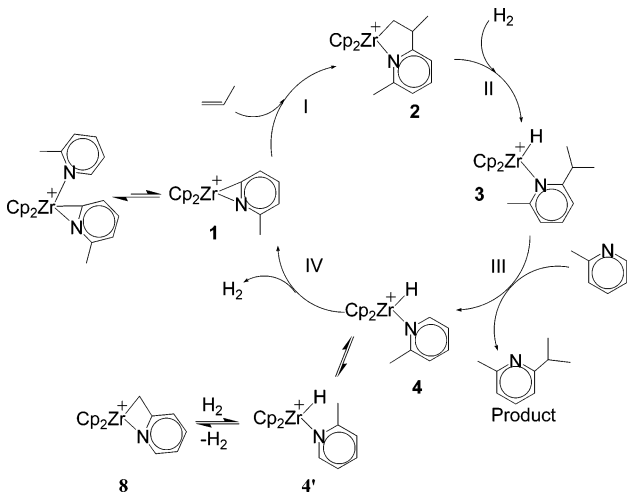

Scheme 3

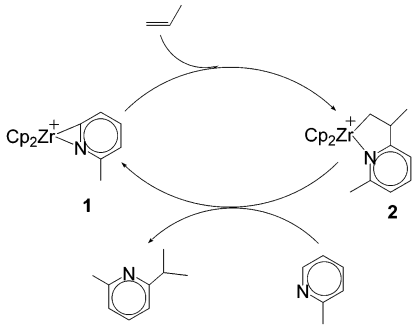

is expected to be ca. 10 kcal/mol stronger than the Zr−C bond that is cleaved.[14,15]

Once **3** is formed, a ligand substitution reaction occurs, leading to the formation of **4** and the release of the disubstituted pyridine product. **4** is more stable than **3** due to the higher steric crowding associated with the 2,6-disubstituted pyridine ligand in **3**. The calculated Zr−N bond in **4** (2.358 Å) is shorter than that in **3** (2.423 Å). Finally, H_2 elimination via the four-center−four-electron transition state **TS6** regenerates **1** and completes the catalytic cycle. The H_2 elimination from **4** is enthapically unfavorable but is driven by the entropy contribution.

The ligand substitution step (**3** → **4**) requires further comment. It is expected that this step will occur through an associative mechanism, as **3** is a 16-electron species. Considering the possibility of the incoming ligand attacking the metal center from different directions, we located two transition states (**TS5a** and **TS5b**). Figure 1c shows the energy profiles for the two directions of attack. In **TS5a** the incoming ligand (picoline) attacks the metal center from the side of the outgoing ligand, while in **TS5b** the incoming ligand (picoline) attacks the metal center from the hydride side. The possibility of the incoming ligand attacking the site between the hydride and outgoing ligand was also considered, but a transition state for this pathway was not found. **TS5a** is calculated to be 3.5 kcal/mol lower in free energy than **TS5b**. It is interesting to note that the Zr- - -N distances in **TS5b** are shorter than those in **TS5a** (Figure 2), while the average Zr−C(Cp) bond distance in **TS5b** (2.59 Å) is longer than that in **TS5a** (2.57 Å). Also, the Zr−H distance (1.796) in **TS5b** is only slightly longer than that in **TS5a** (1.793 Å). Due to the very weak Zr- - -N interactions, the Zr−H distances in these two transition states are shorter than those in **4** and **4′**. These geometric differences between **TS5a** and **TS5b** reflect the balance of interligand steric repulsions and ligand trans influences in these systems. In particular, the trans arrangement of the hydride and 2-Me-picoline ligands results in the short Zr−H and long Zr−N distances in **TS5a**. The difference in the Zr- - -N distances between **TS5a** and **TS5b** probably does not contribute significantly to the relative stability of these transition states, since these bonds are very long. However, the small differences in the Zr−C(Cp) distances between **TS5a** and **TS5b** probably are significant, due to the strength of these bonds. Figure 1c shows that the ligand substitution step requires an activation free energy of 17.74 kcal/mol, lower than that of the olefin insertion step. The entropy contribution for the ligand substitution is very significant (see the reaction energies given in the figure). There are other possible transition structures when one considers different orientations of the N-containing ligands. We did not further consider these structures because they are expected to have greater steric repulsion.

Role of H_2. Comparison of the calculated energy profiles for Scheme 3 (Figure 1a) and Scheme 2 (Figure 1b) provides further insight into the role of H_2 in Scheme 2. Figure 1a shows that the activation free energies for conversion of azazirconacycle **2** to **1** and product via **TS2** and **TS3** are greater than 40 kcal/mol. In contrast, in Scheme 3 the barrier for hydrogenolysis of **2** via **TS4** is only ca. 25 kcal/mol (Figure 1b). Two factors contribute to the difference in these barriers. First, steric interactions between the Cp rings and the other ligands are greater in **TS2** and **TS3** than in **TS4**. This is obvious because in **TS4** the very small hydride ligand replaces a bulky pyridyl ligand. Second, and probably more important, only one hydrogen atom is involved in the four-center−four-electron σ-bond metathesis interaction in **TS2** and **TS3**, while two hydrogens are involved in this interaction in **TS4.** An early study showed that the degenerate transformation of $Cp_2Sc(R^1)(\eta^2\text{-H-}R^2) \rightarrow Cp_2Sc(R^2)(\eta^2\text{-H-}R^1)$ ($R^1 = R^2 = CH_3$) has a barrier of 16.75 kcal/mol, while the transformation of $Cp_2Sc(CH_3)(\eta^2\text{-}H_2) \rightarrow Cp_2Sc(H)(\eta^2\text{-H-}CH_3)$ requires a barrier of only 5.98 kcal/mol.[16,17] It was proposed that the greater overlap associated with the spherical hydrogen 1s orbital compared to the more directional C sp^2 or sp^3 orbitals in such transition states provides enhanced stability.[16,17] In the **TS4** and **TS6** structures, the H1−H2 distances are short (Figure 2), supporting the view that the 1s−1s orbital overlap contributes to the stability of the transition structures.

(14) (a) Crabtree, R. H. *The Organometallic Chemistry of the Transition Metals*, 2nd ed.; John Wiley & Sons: New York, 1994; p 67. (b) Liu, D.; Lam, K. C.; Lin, Z. *Organometallics* **2003**, *22*, 2827.

(15) (a) Labinger, J. A.; Bercaw, J. E. *Organometallics* **1988**, *7*, 926. (b) Schock, L. E.; Marks, T. J. *J. Am. Chem. Soc.* **1988**, *110*, 7701.

(16) Ziegler, T.; Folga, E.; Berces, A. *J. Am. Chem. Soc* **1993**, *115*, 636.

(17) (a) Steigerwald, M. L.; Goddard, W. A., III. *J. Am. Chem. Soc.* **1984**, *106*, 308. (b) Rappe, A. K. *Organometallics* **1990**, *9*, 466. (c) Rabaâ, H.; Sailard, J.-Y.; Hoffmann, R. *J. Am. Chem. Soc.* **1984**, *106*, 4327. (d) Folga, E.; Ziegler, T. *New J. Chem.* **1991**, *15*, 741. (e) Folga, E.; Ziegler, T. *Can. J. Chem.* **1992**, *70*, 333.

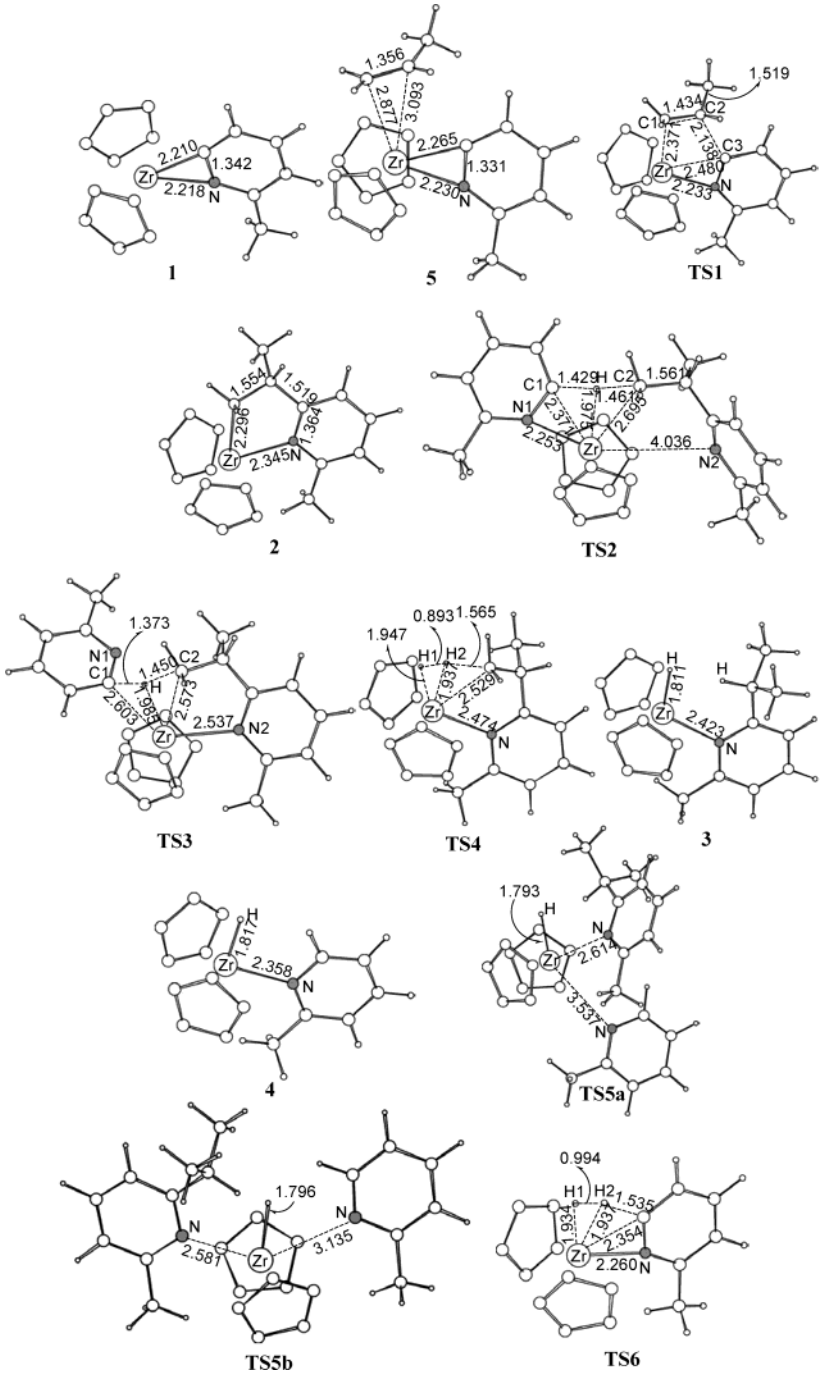

Figure 2. B3LYP optimized structures for those species shown in Figure 1 together with selected bond distances. The bond distances are given in Å. For clarity, the hydrogen atoms on Cp rings are omitted.

Substrate Coordination to 1. It should be noted that the results discussed above are related to the productive part of the catalytic cycle, which emphasizes the role played by the reactive species **1**. Scheme 2 shows that **1** is generated from $[Cp_2Zr(2\text{-Me-6-pyridyl})(2\text{-Me-pyridine})]^+$. To study the feasibility of generating **1**, the 2-Me-pyridine dissociation reaction from $[Cp_2Zr(2\text{-Me-6-pyridyl})(2\text{-Me-pyridine})]^+$ (eq 3) was investigated.

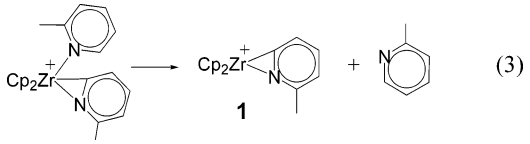

(3)

The 2-Me-pyridine dissociation free energy was calculated to be only 5.04 kcal/mol. The small dissociation free energy is a result of the significant entropy contribution, as the dissociation energy is 22.95 kcal/mol. Experiments showed that $[Cp_2Zr(2\text{-Me-6-pyridyl})(2\text{-Me-pyridine})]^+$ reacts with propene to give **2**.[6] This reaction presumably occurs through the olefin insertion of the propene adduct **5**. Since $[Cp_2Zr(2\text{-Me-6-pyridyl})(2\text{-Me-pyridine})]^+$ is an 18-electron species, its reaction with propene to produce the propene adduct **5**, from which the olefin insertion gives **2**, is reasonably assumed to be dissociative and proceeds via **1**, as shown in Scheme 2. Experimental observations showed that the reaction of $[Cp_2Zr(2\text{-Me-6-pyridyl})(2\text{-Me-pyridine})]^+$ and propene and the reaction of **2** with H_2 are slow compared to the

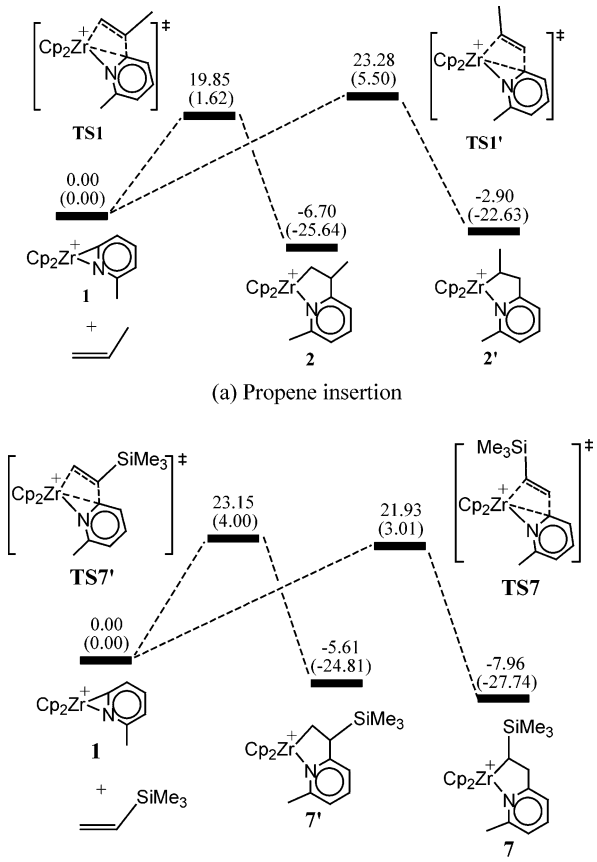

Figure 3. Energy profiles for propene insertion (a) and vinyltrimethylsilane insertion (b) into the Zr−C bond of **1**. The calculated reaction free energies and reaction energies (in parentheses) are given in kcal/mol.

other steps, ligand exchange and H_2 elimination.[6] Taking into account the 2-Me-pyridine dissociation step together with the energy profiles shown in Figure 1b,c, the results of our theoretical calculations agree well with these experimental observations.

Regioselectivity of Olefin Insertion of 1. As noted above, only the Markovnikov C−H addition product was obtained from the reaction of α-picoline with propene (eq 2). The regioselectivity is set at the propene insertion step, which yields the Markovnikov (or "1,2-insertion") product. To understand the origin of the regioselectivity, the reaction of **1** and propene leading to the 2,1-insertion product **2′** (eq 4) was investigated. Hydrogenolysis of **2′** would ultimately yield the anti-Markovnikov C−H addition product 2-Me-6-^{n}Pr-pyridine. The potential energy profiles for the insertions leading to **2** and **2′** are compared in Figure 3a.

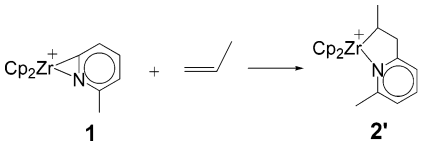

(4)

Consistent with the experimental observations, the formation of **2′** is disfavored relative to the formation of **2**, both kinetically and thermodynamically. The structures of the transition states leading to **2′** (**TS1′**) and **2** (**TS1**) are shown in Figure 4 and Figure 2, respectively. The Zr−C1 bond in **TS1′** (2.458 Å) is much

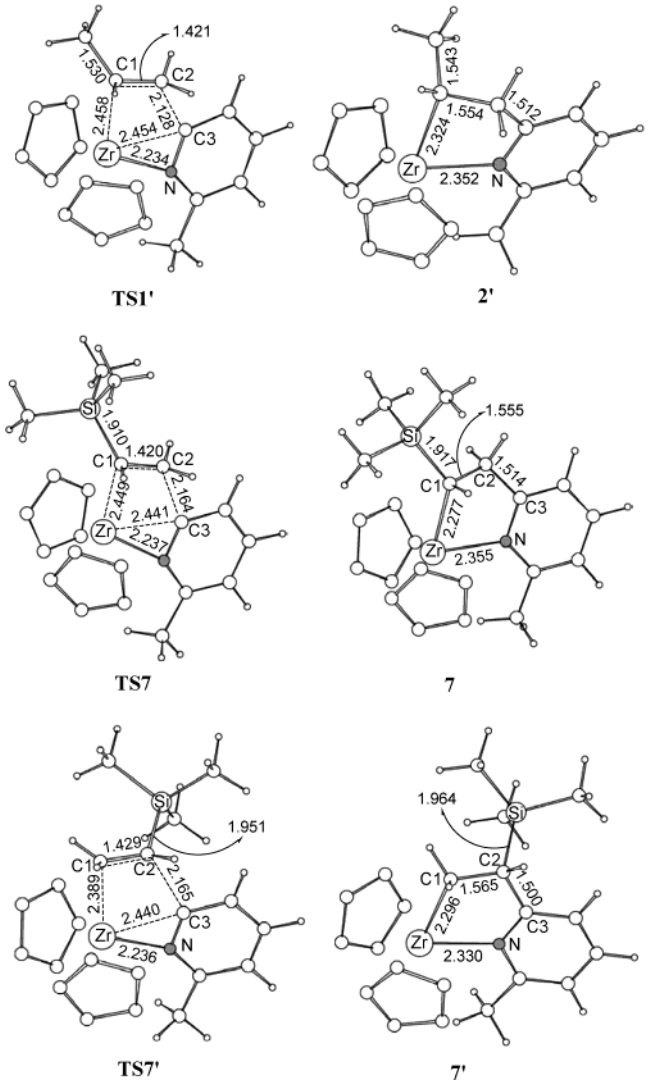

Figure 4. B3LYP optimized structures for those species shown in Figure 3 together with selected bond distances. The bond distances are given in Å. For clarity, the hydrogen atoms on Cp rings are omitted.

longer than that in **TS1** (2.371 Å), due to steric repulsion between a Cp ligand and the propene Me group in **TS1′**. The shortest H- - -H contact in **TS1′** is 2.17 Å between one of the two Cp rings and a propene CH_3 hydrogen, while that in **TS1** is 2.26 Å between one of the two Cp rings and a propene CH_2 hydrogen. These results imply that steric factors control the regioselectivity of propene insertion of **1**.

In contrast to the 1,2 propene insertion, it was found experimentally that vinyltrimethylsilane reacts with **1** to yield the sterically more crowded 2,1-insertion product **7** (eq 5) rather than the less crowded 1,2-insertion product **7′** (eq 6).[18] This result is inconsistent with the steric arguments presented above. Therefore, eqs 5 and 6 were investigated computationally.

Figure 3b shows the potential energy profiles of the insertions leading to **7** and **7′**. The formation of **7** is kinetically and thermodynamically favored over the formation of **7′**. Clearly, electronic effects are important in this case.

(18) (a) Guram, A. S.; Jordan, R. F. *Organometallics* **1990**, *9*, 2190. (b) Guram, A. S.; Jordan, R. F. *Organometallics* **1991**, *10*, 3470.

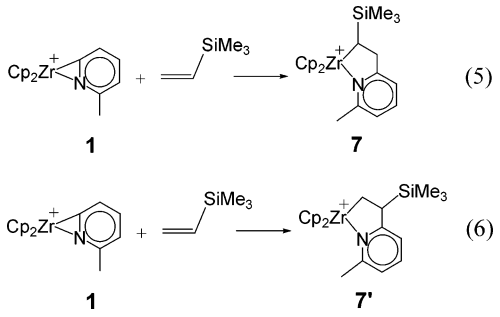

Figure 4 shows the structures of the species in the potential energy profiles in Figure 3b. The Zr−C1 distance in the 2,1-insertion transition state **TS7** (2.449 Å) is longer than that in the 1,2-insertion transition state **TS7′** (2.389 Å), consistent with the anticipated increased steric crowding in **TS7**. However, the difference in the Zr−C1 bond distances between **TS7** and **TS7′** (0.060 Å) is less than that for the propene case (**TS1′** versus **TS1**, 0.087 Å), despite the fact that the $SiMe_3$ group is much larger than a Me group. Further examination shows that the C1−Si bond in **TS7** (1.910 Å) is significantly shorter than that in **TS7′** (1.951 Å), while the remaining bond distances are very similar in the two transition states. Clearly, the stronger C1−Si bonding in **TS7** contributes substantially to the greater stability of **TS7** versus **TS7′**. The short C1−Si bond in **TS7** and product **7** reflects the favorable charge alternation pattern in these species ("charge alternation effect"), due to the 1,3 placement of the electropositive Zr and Si centers.[19,20] Figure 5 shows the atomic charges calculated for these species. The Zr−C1−Si arrangement in **TS7** and **7** shows a charge alternation pattern, while the Zr−C1−C2−Si arrangement in **TS7′** and **7′** does not. These results show that the regioselectivity of vinyltrimethylsilane insertion is controlled by electronic factors.

Activation of α-Picoline Methyl C−H Bonds. As noted above, the only pyridine product observed in eq 2 and Scheme 2 is the disubstituted pyridine derived from activation of the α-picoline ortho C−H bond in intermediate **4**. However, deuterium labeling experiments showed that activation of the α-picoline methyl C−H bonds also occurs and is reversible;[6] that is, as shown in Scheme 2, H_2 elimination from **4′** occurs to give the four-membered ring compound **8**. Products derived from propene insertion of **8** were not observed. To further understand the selectivity observed in eq 2 and Scheme 2, the formation and reactivity of **4′** and **8** were studied computationally.

Energy profiles for the formation and propene insertion of **4** and **4′** are compared in Figure 6. The energies of **4** and **4′** are very similar since no major steric interactions are present. The barrier for activating a methyl C−H bond of **4′** is only ca. 2 kcal/mol higher than that for activating the ortho C−H bond of **4**. However, insertion of propene into **8** via **TS1″** to give **2″** is strongly disfavored relative to insertion of propene into **1** via **TS1** to give **2**. Comparing the structures of **TS1″** (Figure 7) and **TS1** (Figure 2), we find that the Zr−C and Zr−N bond distances are significantly longer in **TS1″**. The formation of a weaker $C(sp^3)-C(sp^3)$ bond in **TS1″** versus the $C(sp^3)-C(sp^2)$ bond in **TS1** and the greater steric crowding in **TS1″** due to the large N−Zr−C1 angle in the metallocene wedge compared to **TS1** contribute to the higher barrier for propene insertion into **8**.

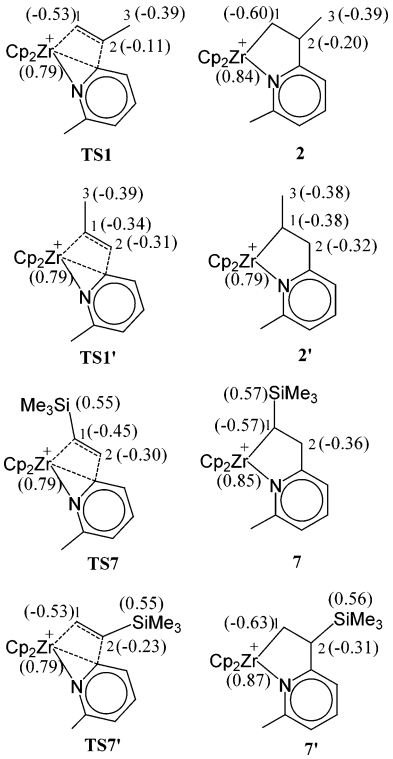

Figure 5. Mulliken atomic charges calculated for those species shown in Figure 3.

Hydrogenation of Propene. It was observed experimentally that minor amounts of propane (ca. 10 mol % versus the disubstituted pyridine product) were formed in eq 2.[6] It is expected that hydride complexes **3** and **4** could catalyze propene hydrogenation via propene insertion to yield Zr-propyl intermediates followed by hydrogenolysis of the Zr-propyl bonds. Figure 8 shows the energy profiles calculated for hydrogenation processes starting from **4**, in which the propene insertion occurs with 1,2 or 2,1 regioselectivity to produce Zr-^{n}Pr or Zr-^{i}Pr intermediates. In both pathways, initial ligand substitution yields a Zr(IV)-propene complex (**9** or **9′**). Subsequent propene insertion into the Zr−H bond yields β-agostic propyl species **10** or **10′**. Coordination of H_2 to **10** or **10′** followed by a σ-bond metathesis and trapping by propene regenerates **9** or **9′** and completes the cycle.

The energy profiles in Figure 8 show that displacement of α-picoline from **4** by propene to yield **9** or **9′** and subsequent propene insertion comprise the rate-determining step. The selectivity for propene/α-picoline coupling over propene hydrogenation results primarily from the fact that Cp_2ZrH^+ binds α-picoline much more strongly than propene. The weak propene coordination in **9** and **9′** results from the absence of d−π* back-bonding in these d^0 metal olefin complexes.[21] The 1,2-

(19) (a) Klein, J. *Tetrahedron* **1983**, *39*, 2733. (b) Becker, J. Y.; Klein, J. *Tetrahedron* **1988**, *44*, 2289. (c) Stolow, R. D.; Samal, P. W.; Giants, T. W. *J. Am. Chem. Soc.* **1981**, *103*, 197. (d) Cohen, Y.; Klein, J.; Rabinovitz, M. *J. Am. Chem. Soc.* **1988**, *110*, 4643. (e) Frenking, G.; Gobbi, A. *Chem. Phys. Lett.* **1992**, *197*, 335.

(20) Lambert, J. B.; Zhao, Y.; Emblidge, R. W.; Salvador, L. A.; Liu, X.; So, J.-H.; Chelius, E. C. *Acc. Chem. Res.* **1999**, *32*, 183, and references therein.

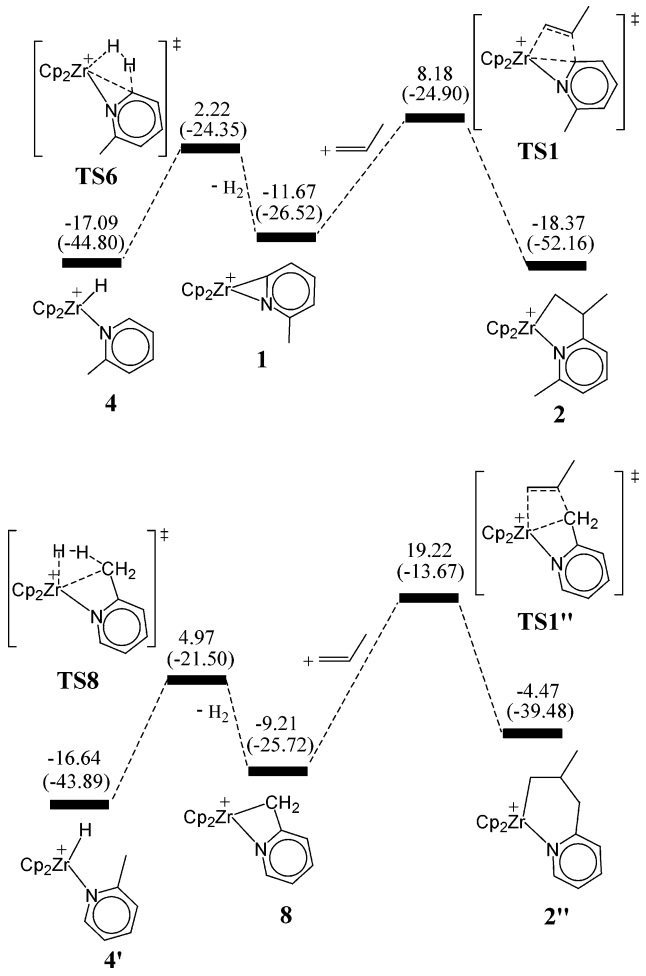

Figure 6. Energy profiles for H_2 elimination from **4** and **4′** followed by propene insertion. The free and reaction energies of **4** are taken from Figure 1b for comparison. The calculated reaction free energies and reaction energies (in parentheses) are given in kcal/mol.

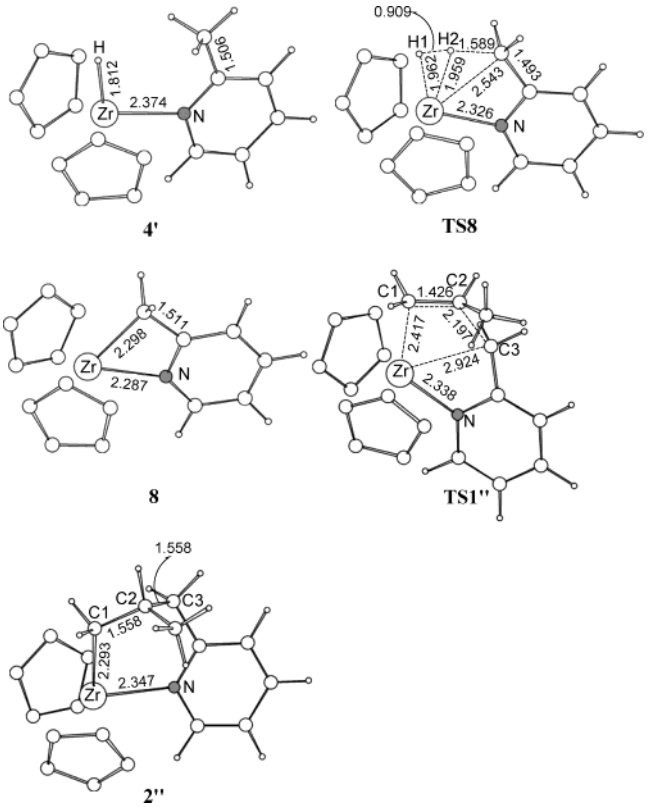

Figure 7. B3LYP optimized structures of **4′**, **TS8**, **8**, **TS1″**, and **2″** together with selected bond distances. The bond distances are given in Å. For clarity, the hydrogen atoms on Cp rings are omitted.

insertion pathway (**TS9**) is slightly favored over the 2,1-insertion pathway (**TS9′**) because placement of the propene methyl group in the center rather than the side of metallocene wedge reduces steric interactions with the two Cp rings.[22]

Conclusions

The mechanism of the Zr-catalyzed addition of the ortho C−H bond of α-picoline to propene has been investigated by DFT calculations. The computational results support the proposed mechanism, which involves (i) 2-Me-pyridine dissociation from $[Cp_2Zr(2\text{-Me-6-pyridyl})(2\text{-Me-pyridine})]^+$ followed by the insertion of propene into the Zr−C bond of the η^2-pyrid-2-yl complex **1** to yield azametallacycle **2**, (ii) σ-bond metathesis by H_2 to produce metal hydride intermediate **3**, (iii) ligand substitution of the disubstituted pyridine ligand of **3** by α-picoline, and (iv) a second σ-bond metathesis to release H_2 and regenerate **1**. Consistent with the experimental results, the 2-Me-pyridine dissociation from $[Cp_2Zr(2\text{-Me-6-pyridyl})(2\text{-Me-pyridine})]^+$ and subsequent propene insertion of **1**, and the hydrogenolysis of **2**, are the rate-determining steps.

The calculations confirm that H_2 plays a crucial role in this catalytic process. In the absence of H_2, a direct α-bond metathesis reaction of **2** and α-picoline might proceed to produce **1** and the disubstituted pyridine product. However, the barrier for this process is inaccessibly high. Introduction of H_2 splits the inaccessible σ-bond metathesis step involving **2** and α-picoline into two accessible σ-bond metathesis steps, one being the hydrogenolysis of **2** by H_2 and the other being the release of H_2 via C−H activation of **4**. The involvement of H_2 makes these four-center transition states energetically accessible because the spherical character of the H 1s orbital increases the orbital overlap and the small size of H alleviates steric crowding.

The Zr-catalyzed addition of the α-picoline ortho C−H bond to propene yields the Markovnikov product. The regioselectivity is set at the propene insertion step, which occurs with 1,2 regioselectivity. Our calculations indicate that steric repulsion between a Cp ring and the propene methyl group inhibits the 2,1-insertion pathway. In contrast, vinyltrimethylsilane inserts into **1** with 2,1 regioselectivity due to electronic effects.

The calculations show that the preference for addition of the α-picoline ortho C−H bond rather than a methyl C−H bond to propene results from the much lower barrier for propene insertion into the η^2-pyridyl species **1** than the four-membered ring compound **8**. Propene

(21) (a) Stoebenau, E. J., III; Jordan, R. F. *J. Am. Chem. Soc.* **2003**, *125*, 3222. (b) Carpentier, J.-F.; Maryin, V. P.; Luci, J.; Jordan, R. F. *J. Am. Chem. Soc.* **2001**, *123*, 898. (c) Carpentier, J.-F.; Wu, Z.; Lee, C. W.; Strömberg, S.; Christopher, J. N.; Jordan, R. F. *J. Am. Chem. Soc.* **2000**, *122*, 7750.

(22) (a) Lantero, D. R.; Ward, D. L.; Smith, M. R., III. *J. Am. Chem. Soc.* **1997**, *119*, 9699. (b) Lantero, D. R.; Miller, S. L.; Cho, J.-Y.; Ward, D. L.; Smith, M. R., III. *Organometallics* **1999**, *18*, 235.

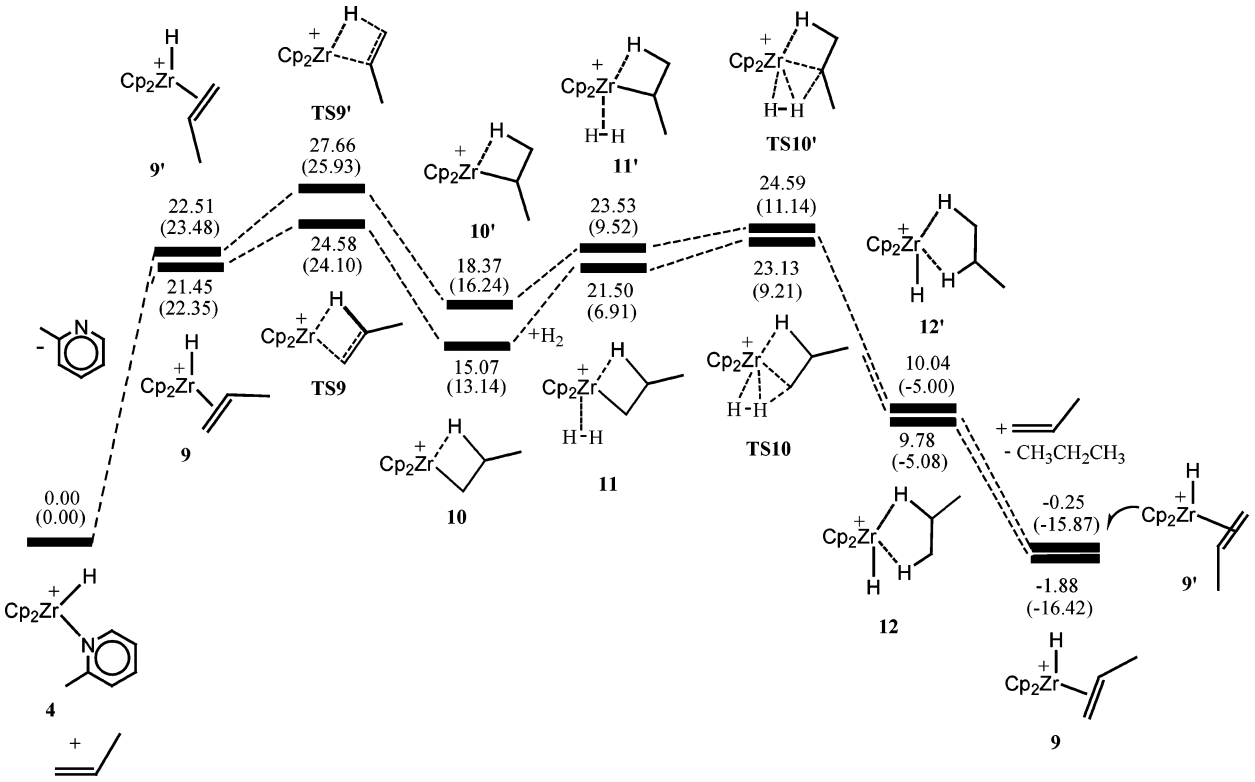

Figure 8. Energy profiles for the hydrogenation of propene. The calculated reaction free energies and reaction energies (in parentheses) are given in kcal/mol.

insertion into **1** is favored because this reaction forms a $C(sp^3)-C(sp^2)$ bond, while reaction with **8** generates a $C(sp^3)-C(sp^3)$ bond, and because steric crowding in the insertion transition state from **1** is much less than that from **8**. The preference for α-picoline/propene coupling over propene hydrogenation results from the much stronger binding of α-picoline versus propene to the Cp_2ZrH^+ intermediate.

Acknowledgment. This work was supported by the Research Grant Council of Hong Kong (HKUST 6087/02P and DAG03/04.SC15), the University Grants Committee of Hong Kong through the Area of Excellence Scheme (Aoe), and the U.S. National Science Foundation (CHE-0212210).

Supporting Information Available: Cartesian coordinates of all the calculated structures reported in this article are available free of charge via the Internet at http://pubs.acs.org.

OM0496784